ELECTRONIC SUPPLEMENTARY INFORMATION

UVC-Induced Valence Switching in BaFBr:Sm^{3+} Nanoplates

Nishani T. Manamperi and Federico A. Rabuffetti*

Department of Chemistry, Wayne State University, Detroit, MI 48202, USA

*Corresponding Author. Email: far@chem.wayne.edu

Table S1. Refined Structural Parameters of BaFBr:Sm^{3+}

a (Å)	4.4945(5)
c (Å)	7.4863(19)
V ($Å^3$)	151.23(6)
*z*Ba	0.1943(4)
*z*Br	0.6468(7)
Ba–F (Å)	2.6769(17) (×4)
Ba–Br (Å)	3.393(3) (×4), 3.388(7) (×1)

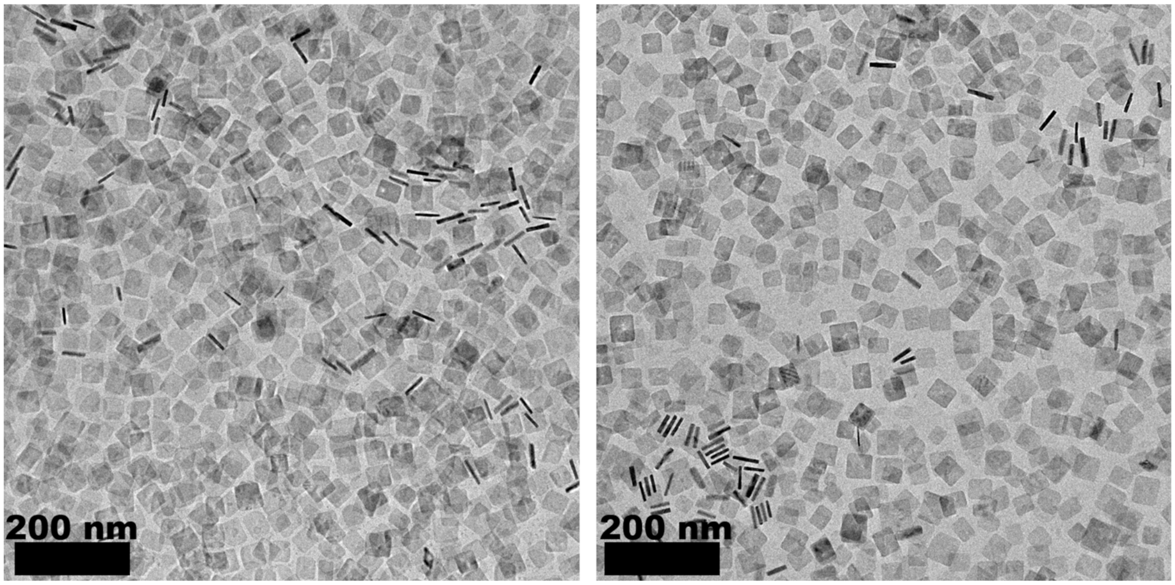

Figure S1. Additional TEM images of BaFBr:Sm^{3+} nanoplates.

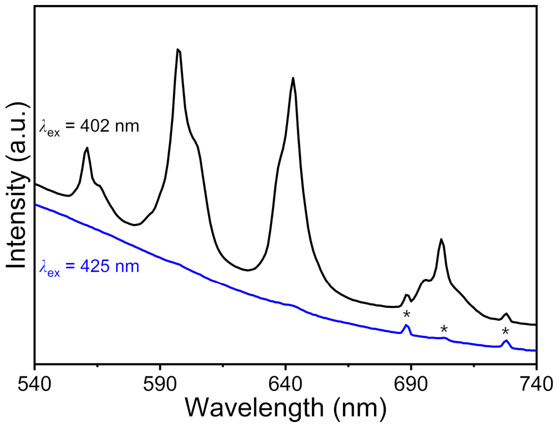

Figure S2. Emission spectra of BaFBr:Sm^{3+} after short exposure (ca. 3 min) to 250 nm UVC radiation. Peaks corresponding to photogenerated Sm^{2+} are marked with the * symbol.

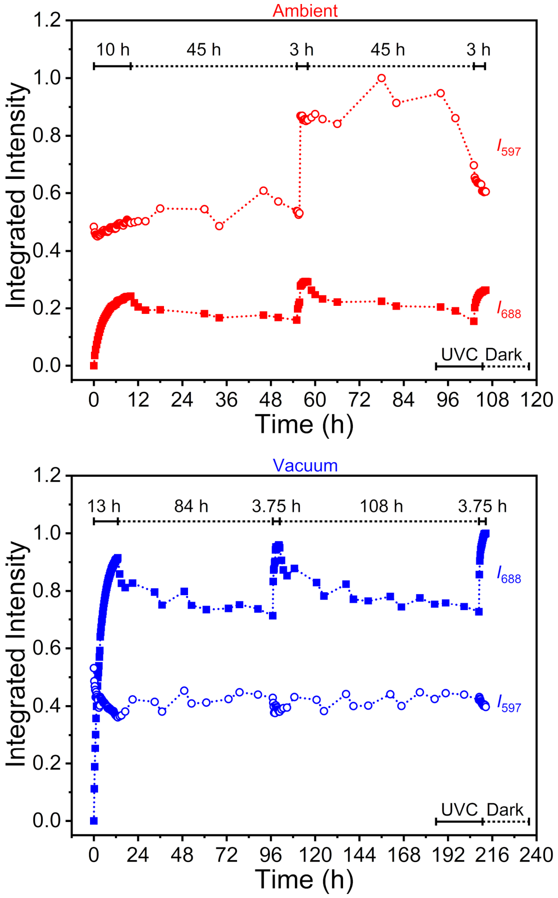

Figure S3. Time evolution of integrated emission intensities I_{597} (Sm^{3+}) and I_{688} (Sm^{2+}) during UVC–dark cycling under ambient atmosphere (top panel) and under vacuum (bottom panel). Intensities are normalized with respect to their maximum values (I_{597}(78 h) under ambient atmosphere and I_{688}(212.5 h) under vacuum). Dotted lines are guides to the eye.

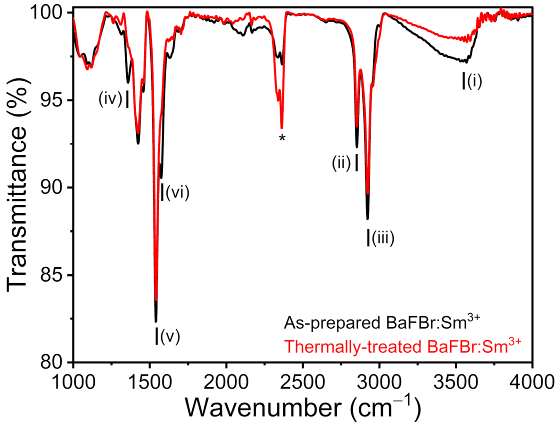

Figure S4. Infrared spectra of as-prepared and thermally-treated BaFBr:Sm^{3+}. Thermal treatment entailed heating under vacuum at 450 K for 6 h and induced partial dehydration of the nanoplates' surfaces as well as removal of residual organic ligands. Dehydration led to a decrease in the intensity of the broad band arising from stretching vibrations of hydrogen-bonded hydroxyl groups (band (i) at 3044–3684 cm^{-1}). Likewise, the decrease in the intensity of the bands belonging to stretching vibrations of aliphatic hydrocarbons resulted from removal of organic ligands (band (ii) at 2851 cm^{-1} and (iii) at 2924 cm^{-1}). Removal of residual organics also led to a decrease in the intensity of the bands arising from stretching vibrations of carboxylate groups (band (iv) at 1357 cm^{-1}, (v) at 1541 cm^{-1}, and (vi) at 1575 cm^{-1}). Spectra were recorded using a Fourier transform infrared spectrophotometer (IRTracer–100, Shimadzu Corporation) equipped with a single-reflection attenuated total reflectance accessory. For each sample, 300 scans were collected between 1000 and 4000 cm^{-1} with a resolution of 4 cm^{-1}. The band denoted with the * symbol corresponds to atmospheric CO_2.

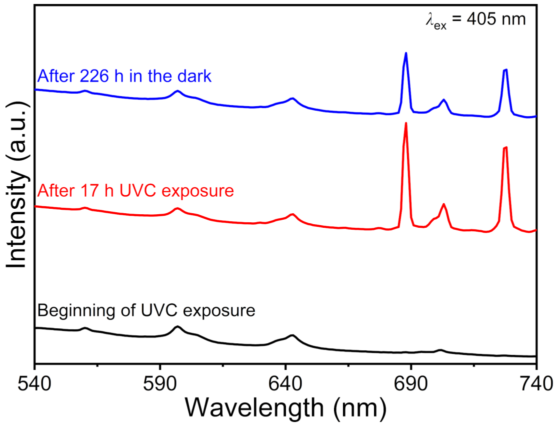

Figure S5. Selected emission spectra collected in the course of kinetic studies. Spectra corresponding to nanocrystals at the beginning of UVC exposure, at the end of the UVC stage, and at the end of the dark stage are shown.

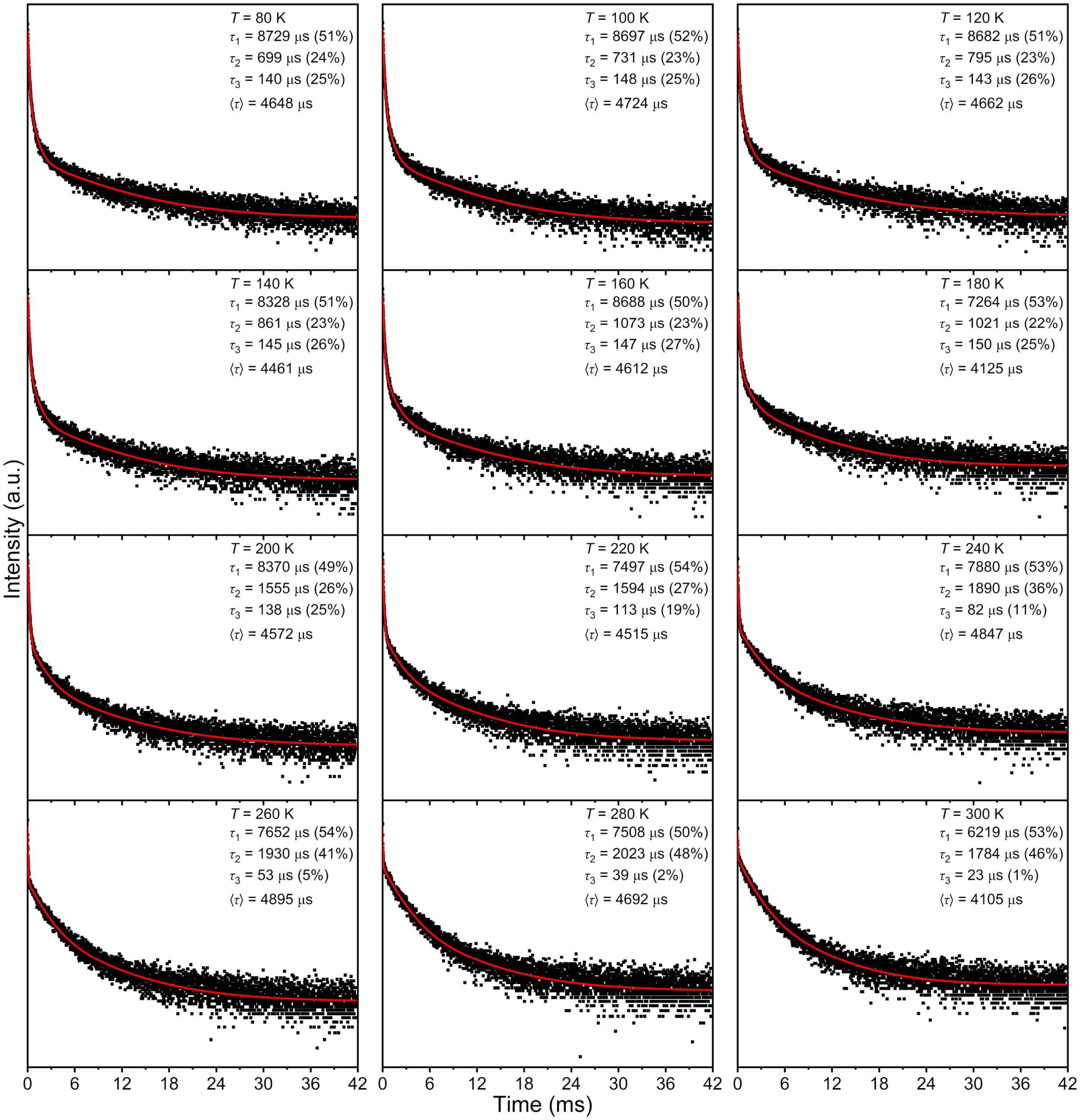

Figure S6. Variable-temperature time-resolved luminescence decays of BaFBr:Sm$^{2+/3+}$. Decays were excited at 405 nm and monitored at 629 nm (Sm^{2+} $^5D_1 \rightarrow {}^7F_0$). Triexponential fits are shown as solid red lines. Individual lifetimes and intensity-weighted average lifetimes are given along with fractional contributions. All decays are shown in logarithmic scale.

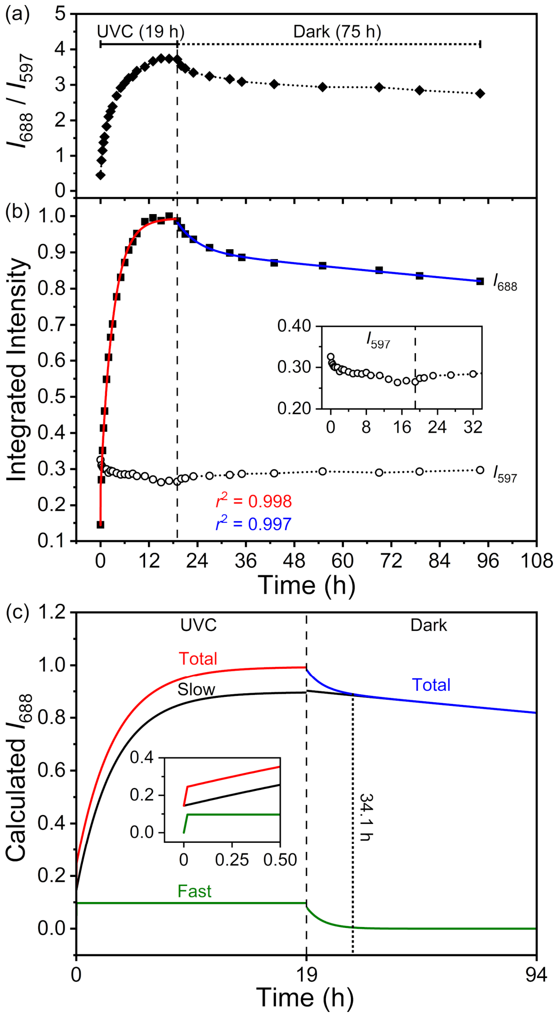

Figure S7. Kinetics of UVC photoreduction and dark ionization of BaFBr:Sm^{3+} thermally treated under vacuum. Time evolution of the luminescence intensity ratio (a) and of the corresponding integrated intensities I_{597} and I_{688} (b). A magnified view of the $I_{597}(t)$ curve is shown in the inset. Fits of equations 2 and 3 to the $I_{688}(t)$ curve are shown as solid red and blue lines, respectively. Parameter values extracted for the photoreduction stage were $a = 0.850(6)$, $f = 0.89(1)$, $k_1 = 0.32(1)$ h^{-1}, and $k_2 = 7.78 \times 10^8$ h^{-1}. Values for the dark stage were $a = 0.984(3)$, $f = 0.083(6)$, $k_1 = 0.19(3)$ h^{-1}, and $k_2 = 0.00126(9)$ h^{-1}. Fit residuals are given. (c) $I_{688}(t)$ curve calculated according to equations 4a,b (UVC stage) and 5a,b (dark stage). Contributions from slow and fast components to the total intensity are plotted. A magnified view of $I_{\text{slow}}(t)$, $I_{\text{fast}}(t)$, and $I_{\text{total}}(t)$ curves in the first 30 min of UVC exposure is shown in the inset. Nanocrystals used in this experiment had been previously exposed to UVC radiation and, as a result, $I_{688}(0) \neq 0$. That constant was included in equation 2 prior to fitting experimental data. Likewise, it was included in equation 4a used in the calculation of the contribution of the slow component (i.e., we assumed that the initial emission intensity was entirely due to the slow component). Dashed and dotted lines are guides to the eye.

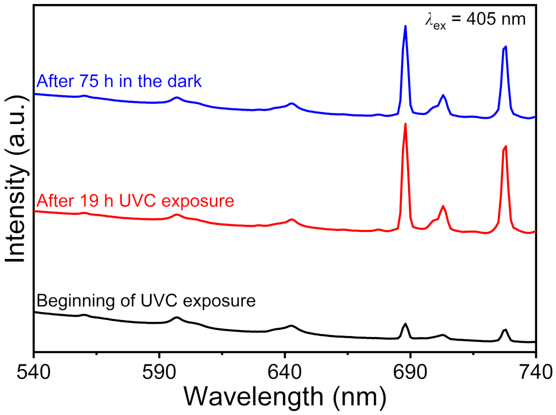

Figure S8. Selected emission spectra collected in the course of kinetic studies of BaFBr:Sm^{3+} thermally treated under vacuum. Spectra corresponding to nanocrystals at the beginning of UVC exposure, at the end of the UVC stage, and at the end of the dark stage are shown. Nanocrystals used in this experiment had been previously exposed to UVC radiation and, as a result, $I_{688}(0) \neq 0$ ($I_{688}/I_{597}(0) \approx 0.44$)

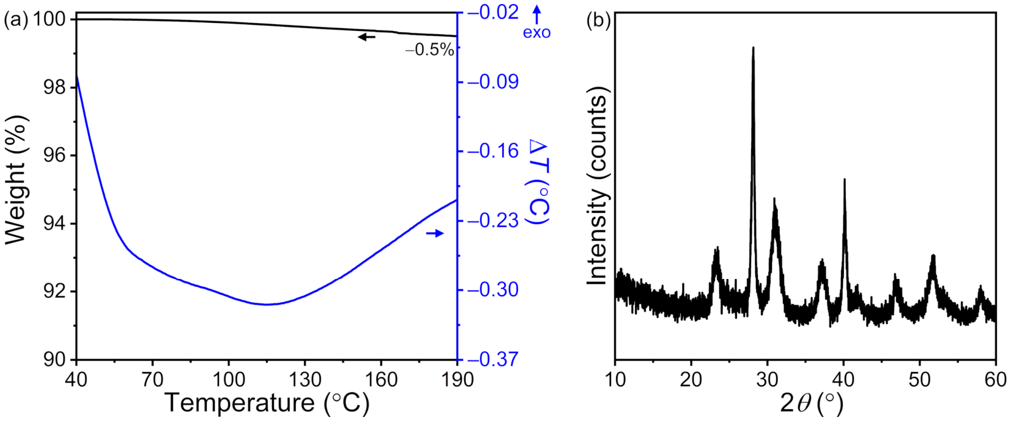

Figure S9. (a) Thermogravimetric (TGA) and differential thermal (DTA) analysis of BaFBr:Sm^{3+}. Thermal analysis was conducted under flowing nitrogen (100 mL min^{-1}) using a TGA–DTA analyzer (SDT2960, TA Instruments). ≈10 mg of sample were placed in an alumina crucible, held at 35 °C for 10 min, ramped to 200 °C at a rate of 10 °C min^{-1}, and kept at that temperature for 15 min. Total weight loss is indicated. (b) Post-thermal analysis PXRD pattern collected in the 10–60° 2*θ* range using a step size and time equal to 0.012° and 0.25 s, respectively.

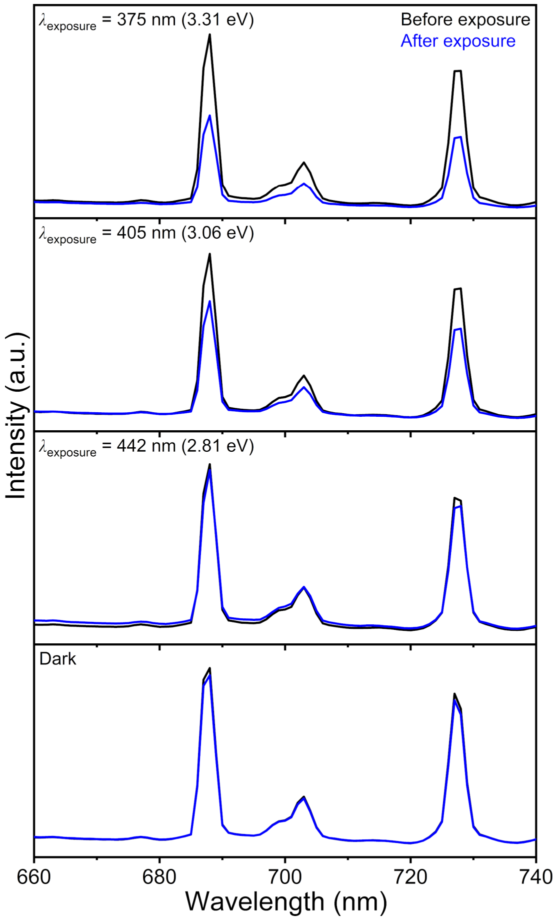

Figure S10. Raw emission spectra of BaFBr:Sm$^{2+/3+}$ before and after exposure to laser light of wavelength $\lambda_{\text{exposure}}$. Spectra were collected using 405 nm excitation.

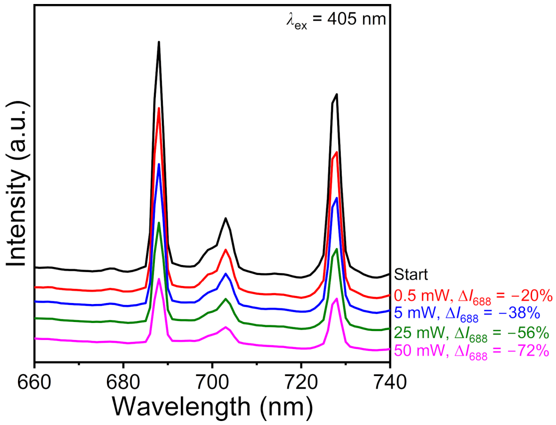

Figure S11. Emission spectra of BaFBr:$Sm^{2+/3+}$ before and after sequential exposure to 405 nm laser light of increasing power. BaFBr:Sm^{3+} nanocrystals thermally treated under vacuum were first exposed to UVC radiation to generate Sm^{2+} ($I_{688}/I_{597} \approx 2.79$), and then continuously to laser light of a given power for 2 h (0.5, 5, 25, and 50 mW). Emission spectra after laser exposure were collected using 405 nm excitation (0.5 mW). The percent change of Sm^{2+} emission intensity at 688 nm (ΔI_{688}) is given.